Check for updates

Improvement in the healing of bone fractures using a cyclodextrin/Ni-MOF nanofibers network: the development of a novel substrate to increase the surface area with desirable functional properties

Junfei Lin,†[a] Chenyu Zong,†[a] Baisen Chen,[b] Teng Wang,[c] Jiacheng Xu,[a] Jiashang Du,[a] Yinghao Lin,[a] Yuming Gu[a] and Jianwei Zhu [ID] *[a]

In this study, a β-cyclodextrins (β-CDs)/Ni-based MOF (β-CDs/Ni-based MOF) fibrous network with focus on biocompatible and biodegradable properties was used as a new material for orthopedic applications. The final products were synthesized by an efficient, rapid, and controllable electrospinning route under optimal conditions, including a flow rate of 0.3 mL g^{-1}, applied voltage of 18 kV, and spinning distance of 20 cm. Efficient characterization by various analyzes showed that the β-CDs/Ni-based MOF fibrous nanostructures had a thermal stability at about 320 °C and homogeneous particles with a narrow size distribution. The BET analysis results showed a specific surface area of 2140 m^2 g^{-1} for these compounds, which facilized potential conditions needed for the application of these compounds as a new substrate to improve the healing of bone fractures. The results showed the better porosity of the β-CDs/Ni-based MOF scaffolds as an essential property, leading to higher proliferation and nutrition and oxygen delivery, resulting in more tissue regeneration. This study proposes a novel strategy for a fibrous network substrate with distinct properties for orthopedic purposes.

1. Introduction

Bone tissue engineering has aroused considerable attention recently as a successful approach for bone regeneration and repair. Bone engineering can meet a number of requirements by selecting a cell type capable of maturing or differentiating into bone cells with a controllable phenotype, regulating growth factors, and providing an optimal scaffold.[1] A scaffold is considered ideal when both the degraded and bulk forms are biocompatible or when it can be represented by an inter-connected and permeable porous structure to allow cells to penetrate while it must also contain nutrients with good chemistry and surface structure for the proliferation and adhesion of cells. Efforts have been made to build scaffolds capable of mimicking the architecture used in the naturally occurring extracellular matrix (ECM). A variety of protein fibrils and fibers form the naturally occurring ECM, which takes the form of a hydrated network of intertwined glycosaminoglycan and collagen chains. This network structure in the scaffold is able to withstand compressive and tensile stresses by relying on hydrated networks and fibrils. The ECM not only provides a suitable cell microenvironment, but also enables the trans-mission of signals to cell membrane receptors, eventually reaching the nucleus through intracellular signaling cascades. Thus, the porous and fibrillar architecture enables the ECM to improve cell function, especially adhesion, migration, and proliferation.[2–4]

One recent strategy for mimicking the structure of a natural ECM is through electrospinning processes using nanofibers. Some applications of this approach are in the production of nanofibrous structures using synthetic and natural polymers such as polycaprolactone, polyurethane, poly(lactide), poly(DL-lactide-co-glycolide), silk fibroin, chitosan, and collagen.[5–11] In addition, it is possible to control the rate of system degradation by combining natural and synthetic polymers.[12–15] For example, increasing the natural polymer content increases the degrada-tion kinetics of a biosynthetic compound. The rate of scaffold degradation can be matched to the growth rate of the regener-ating tissue through appropriate mixture composition. Various tissues, which can be engineered by fabricating polymeric nanofibrous networks, have been proposed.[16–18] In a study by Li *et al.*, chondrocyte proliferation was enhanced and the chon-drogenic phenotype could be maintained through a fabricated biocompatible electrospun polycaprolactone (PCL) membrane.[19]

[a]*Department of Orthopedics, Affiliated Hospital of Nantong University, Nantong, Jiangsu, China. E-mail: zhujianweint@126.com; 2113320256@stmail.ntu.edu.cn; 2013320205@stmail.ntu.edu.cn*

[b]*Department of Orthopedics, Nantong First People's Hospital, Nantong, Jiangsu, China*

[c]*Department of Bioinformatics, School of Basic Medical Sciences, Chongqing Medical University, Chongqing, China*

† First author and Co-first author: Junfei Lin and Chenyu Zong contributed the equal work.

Cyclodextrins (CDs) are natural cyclic oligosaccharides that consist of glucose units. Among these, special attention has been paid toward β-cyclodextrin (β-CD), whose cycle has seven glucose units, owing to its high availability. CDs are strongly able to accept lipophilic compounds in their cavity in an aquatic medium, which makes them a suitable candidate for the construction of optimized engineering scaffolds.[20,21] Supramolecular three-dimensional (3D) scaffolds were constructed using β-CD-anchored polymers.[22,23] β-CDs have been widely applied in biomedical engineering due to their superior properties, namely excellent biocompatibility, bioresorbability, hemocompatibility, bioactivity, mechanical flexibility, non-toxicity, and easy processability. Tissue engineering can show a performance enhancement when using β-CD-anchored scaffolds through increasing the oxygen content in tissue engineered architectures, sequestering the growth factors, and regulating collagen self-assembly.[24–27] Such scaffolds are also capable of releasing drugs within cell cultivation.[28] Nevertheless, one key weakness is their small surface area. This bottleneck may be circumvented by utilizing the fibrous composites of this polymer *via* porous compounds, such as carbon nanostructures, metal–organic frameworks (MOFs), and zeolites.[29]

The strong interplay of organic linkers and metal ions can lead to the fabrication of MOFs with 3D crystalline structures, ultrahigh porosity, and regular pores.[30,31] Such admirable properties have made MOFs widely used candidates for building sensors, catalysts, and medical devices, as well as for gas separation.[32–34] Some of techniques used for the fabrication of MOFs include mechanochemical, electrospinning, sono-chemical, solvochemical, and electrochemical procedures. Evidence suggests that the porosity of polymer fiber mats can be increased by augmenting them with MOFs as compounds with a highly porous structure. Composites of such porous materials typically contain nanostructures or microstructures of MOFs that are blended in a polymer matrix with fibrous or monolithic shapes.[35–37]
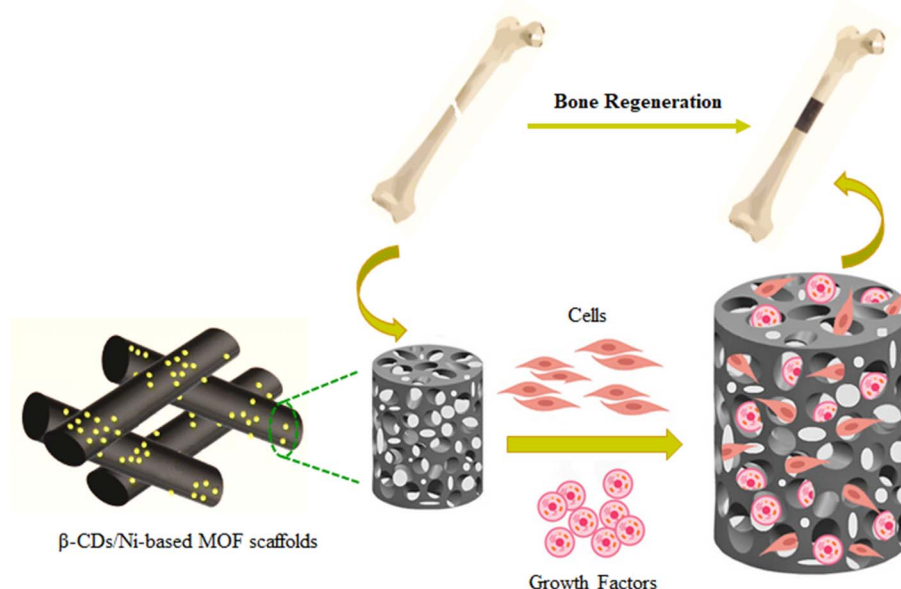
The present work aimed to fabricate and characterize a new composite scaffold composed of β-cyclodextrins (β-CDs)/Ni-based MOF (β-CDs/Ni-based MOF). It was hoped an admirable template could be achieved for osteogenesis by combining β-CDs and a Ni-based MOF, which could further contribute to the successful development of composite scaffolds for bone regeneration and repair (Scheme 1).

2. Experimental

2.1. Materials and apparatus

All the chemicals used in this study were obtained from Merck or Sigma Aldrich, with high purity and without any further purification needed.

Fourier transform infrared spectroscopy (FT-IR; SHIMADZU FT8400 spectrometer) was performed with a Bruker Tensor 27 series for determination of the vibrational frequency of the prepared samples in the range of 400 and 4000 cm^{-1}. The β-CDs/Ni-based MOF composites were examined for their crystallite size, phase structure, and crystallinity using a Philips PC-APD X-ray diffractometer and Kα radiation (α_2, $\lambda_2 = 1.54439$ Å) and graphite mono-chromatic Cu radiation (α_1, $\lambda_1 = 1.54056$ Å) (the Netherlands). The data were analyzed by X'Pert HighScore Plus software. The captured XRD patterns were within 2θ values of 2° to 80° with a step size of 0.016°. The β-CDs/Ni-based MOF composites were morphologically explored by scanning electron microscopy (SEM) and energy dispersive spectrometry (EDS) (KYKY & EM 3200). Transmission electron microscopy (TEM) was performed using an H-7500 transmission electron microscope (Hitachi, Japan). A STA-1500 Thermal Analyzer was employed to analyze the thermal behavior in N$_2$ in the range of

Scheme 1 Schematic bone tissue engineering process.

ambient temperature up to 350 °C. Magnetization measurements were carried out with a Lakeshore system (model 7407) under magnetic fields at room temperature.

The tensile properties of the electrospun fiber scaffolds were determined with a tabletop MicroTester (Instron 5845, USA) using a low force load cell with a capacity of 10 N. Strip-shaped specimens (30×6 mm^2) were tested at a crosshead speed of 10 mm min^{-1}. Ambient conditions were controlled at 25 °C and humidity at 74%. At least six samples were tested for each type of electrospun fibrous scaffold. The ultimate strength, Young's modulus, and tensile elongation were calculated based on the generated tensile stress–strain curves.

2.2. Fabrication of the β-CDs/Ni-based MOF composite

The Ni-based MOF samples were synthesized as per the following: In a 150 mL glass beaker, 4.8 mmol of Ni(NO$_3$)$_2$·6H$_2$O and 0.9 mmol of polyvinylpyrrolidone (PVP) were dissolved in 80 mL of ethanol (Sol. A). In a 100 mL glass beaker, 1.7 mmol of pyridine-2,6-dicarboxylic acid (pyridine 2,6-dicarboxylic acid was formed as pyridine 2,6 diammonium acetate) was dissolved in 30 mL of ethanol (Sol. B). For conventional solvothermal crystallization, the resultant solution (Sols A and B) was transferred into a Teflon reactor with a tight cap and kept at 80 °C for 7 h. For ultrasonic synthesis, however, Sols A and B were transferred into a Teflon reactor and irradiated in the ultrasonic bath for specific sonication time at the predetermined temperature. The resulting product was filtered, washed, and dried at 80 °C for 7 h.[38]
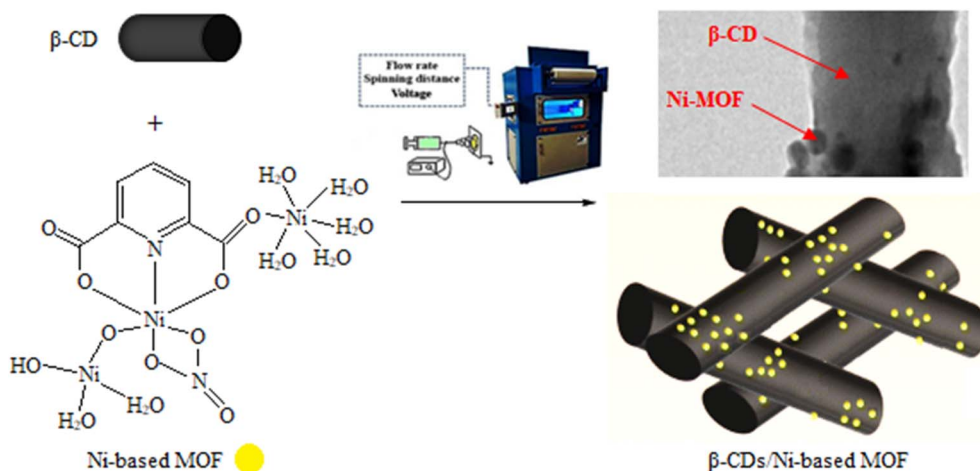
A routine electrospinning process was carried out by blending 2 mg of Ni-MOF and 5 mg of β-CDs powder (Merck) in acetic acid (Aldrich) in a glass vial, followed by stirring vigorously at 70 °C for 40 min. Then, electrospinning was performed under mild circumstances including 20% humidity and at 30 °C. The optimized circumstances for the electrospinning included a voltage of 20 kV and spinning distance of 8 cm. The Ni-based MOF concentration was kept constant at 10 wt% with a flow rate of 0.16 mL h^{-1}. Scheme 2 shows a schematic representation of the β-CDs/Ni-based MOF composite.

2.3. *In vitro* biocompatibility

To observe the adhesion behavior of MC3T3-E1 osteoblasts on the Ni-based MOF and β-CDs/Ni-based MOF membranes, circular specimens of 3 mm diameter dimensions were prepared. Briefly, the samples were fitted in a 96-well microplate culture dish and subsequently sterilized with 70% ethanol for 30 min. The specimens were again washed twice with PBS solution, and once with 70% ethanol, and then dried as much as possible. Next, 100 μl of MC3T3-E1 cell solution containing 1 $\times 10^3$ cells was seeded on each sample well on a microplate and incubated for 3 days to observe the cell line interactions with the nanofibrous membranes. After incubation, 4% paraformaldehyde phosphate buffer solution was added and kept at 4 °C for 4 h to fix the cells with the membranes. After that, the specimens were refrigerated for 1 h and then washed 3 times with PBS solution. After successive washing with ethanol, 50 μl butyl alcohol was added to each specimen and refrigerated for 1 day. Finally, all the specimens were freeze-dried for 12 h. One-way ANOVA and Tukey *post hoc* tests were used to analyze multiple comparison pairs, at a significance level of $p < 0.05$ and $n = 4$ for all circumstances.

2.4. Cell culturing

Normal human dermal fibroblasts (NHDF) as a representative of primary mature mesenchymal cells were used to analyze the possible effects of β-CDs/Ni-based MOF on cell viability. The cell line of NHDF was selected for *in vitro* testing of the planar fibrous materials, provided by ATCC (LGC Standards; Lomianki; Poland). The cell culture was done in fibroblast growth medium-2 (FGM-2, BulletKit™ from Lonza, Basel, Switzerland) with 5% CO$_2$ at 37 °C. The materials were sectioned into 10 mm round samples, followed by sterilization *via* 70% ethanol for half an hour and washing thoroughly in phosphate-buffered saline (PBS, pH 7.4) prior to cell culture. The NHDF cells were implanted in the eighth passage (2000 cells per well) on the material surface. The material–cell interplay was explored on days 1, 6, and 12 after incubation. A cell counting test (cck-8,

Scheme 2 Synthesis rote for preparation of the β-CDs/Ni-based MOF composite.

Merck) was utilized to determine the cell viability, so that 250 L of 10% cck-8 solution (in FGM-2 medium) was appended to each sample and incubated with 5% CO_2 at 37 °C for 3 h. The optical density (OD) was read at 450 nm *versus* 650 nm (a reference wavelength). The fibroblasts were visualized by fluorescence staining. The specimens were rinsed with PBS (pH 7.4) twice, and then fixed by 2.5% glutaraldehyde in PBS at 4 °C for half an hour. Subsequently, the specimens were rinsed with PBS, and stained by 4′,6-diamidino-2-phenylindole (DAPI, Merck) plus fluorescein isothiocyanate-labeled phalloidin (phalloidin-FITC) (Merck). Next, the cells were exposed to Triton (0.1%, Merck) for permeability testing, followed by rinsing in PBS and incubating with exposure to phalloidin-FITC (1 mg per mL stock solution diluted in PBS as 1 : 1000) for half an hour at ambient temperature. Afterward, the specimens were rinsed in PBS and incubated with exposure to DAPI for 5 min at ambient temperature. Finally, the specimens were rinsed in PBS and observed *via* a NICON Eclipse Ti-e fluorescent microscope.

3. Result and discussion

3.1. Characterization of the β-CDs/Ni-based MOF composite

A variety of methods, including XRD, FT-IR, EDS-mapping, FE-SEM, BET, and TGA, were employed to characterize the β-CDs/Ni-based MOF composites. Fig. 1 illustrates the FT-IR spectra captured for the β-CDs nanofibers and β-CDs/Ni-based MOF fibrous fabricated *via* the electrospinning process. According to the FT-IR spectrum for the β-CDs, there were characteristic peaks observed at 3077 to 3317 cm^{-1} belonging to O–H group stretching. The peak at 2850 cm^{-1} was related to C–H symmetric/asymmetric stretching vibration. Moreover, the 1653 cm^{-1} band related to H–O–H deformation of water in β-CD. In addition, the peaks at 1161 and 1012 cm^{-1} corresponded to C–H overtone stretching vibrations and the peak at 1012 cm^{-1} to C–H, C–O stretching vibration. There was also a peak at 1161 cm^{-1} belonging to the absorption of C–O–C vibration.[39] According to the FT-IR spectrum for the β-CDs/Ni-based MOF composite, all the peaks corresponding to the β-CDs and Ni-based MOF were still there in the final structure of

the β-CDs/Ni-based MOF specimen, strongly confirming the successful fabrication of the polymeric fibrous composite.

Fig. 2 illustrates the XRD patterns obtained for the β-CD and β-CDs/Ni-based MOF composite. Fig. 5a shows the amorphous nature of β-CD, while Fig. 5b shows the crystalline form of the Ni-based MOF. Based on the XRD pattern (Fig. 5c) for the physical mixture, both species were present as isolated solids, because the diffractogram exhibited both Ni-based MOF peaks and the β-CD amorphous halo. Scherrer's eqn (1) was used to determine the crystallite size of the as-fabricated β-CDs/Ni-based MOF composite.

$$D = \frac{0.9\lambda}{\beta \cos \theta} \qquad (1)$$

where, λ indicates the X-ray wavelength (1.54056 Å for Cu lamp), β refers to half the width of the maximum intensity diffraction peak, and θ means half the Bragg diffraction angle.[40] The average crystallite size was estimated to be 132.4 ± 0.02 nm for the β-CDs/Ni-based MOF composite and 130.6 ± 0.01 nm for the β-CDs.

Fig. 3 illustrates the SEM images captured for the β-CDs/Ni-based MOF composite and β-CDs. Fig. 3a shows the continuous and cylindrical morphology of the β-CDs fibers with a mean diameter of 165 nm. Fig. 3b confirms the unchanged shape of the β-CDs nanofibers during the composite fabrication. As can be observed, the Ni-based MOF composite had been embraced by the β-CDs matrix. Fig. 3c shows the TEM image of the β-CD/Ni-based MOF composite, which confirmed its fibrous morphology with an average fiber diameter of 600 nm for this compound. According to Fig. 3c, Ni-based MOF particles had agglomerated onto the surface of the β-CD nanofibers. In
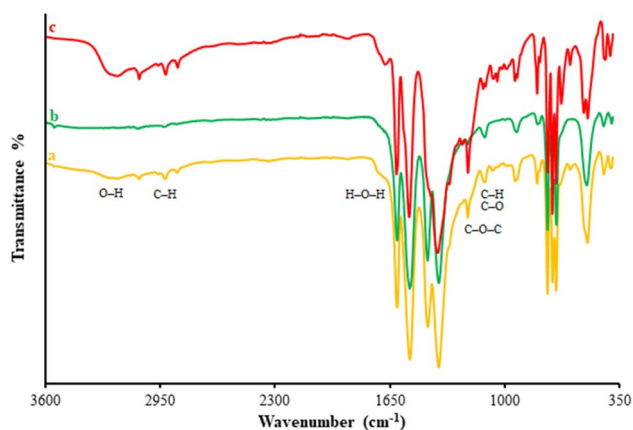

Fig. 1 FT-IR spectra of β-CDs (a), Ni-based MOF (b), and β-CDs/Ni-based MOF composite (c).
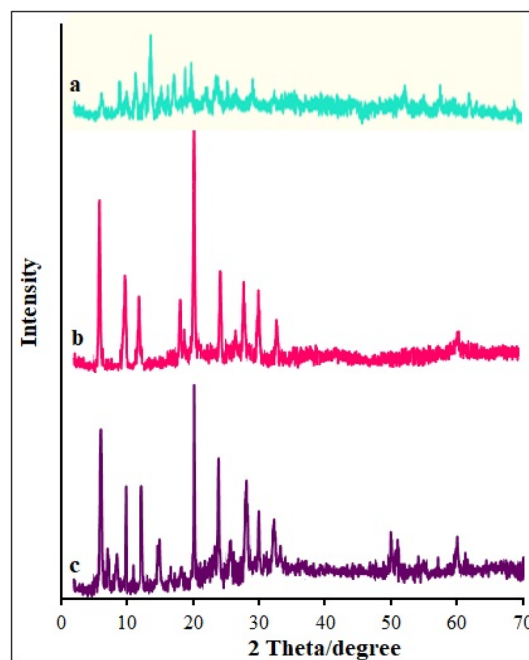

Fig. 2 XRD patterns of β-CDs (a), Ni-based MOF (b), and β-CDs/Ni-based MOF composite (c).
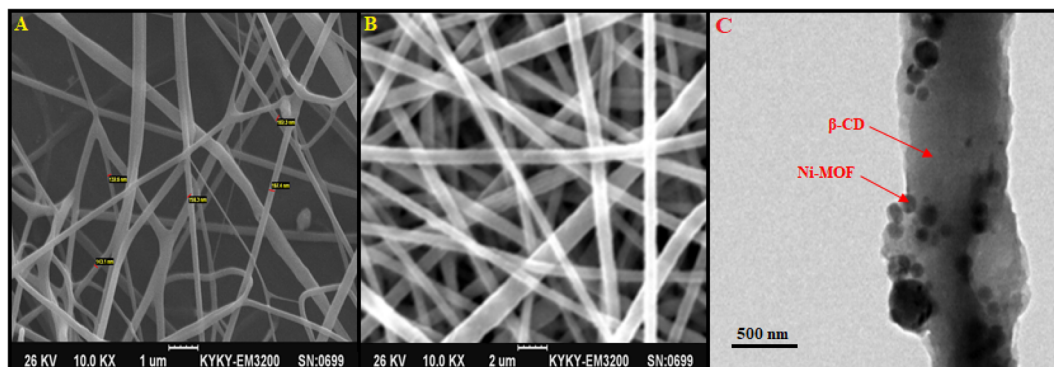
RSC Advances

Paper

Fig. 3 SEM images of β-CDs (A), β-CDs/Ni-based MOF composite (B), and TEM image of β-CDs/Ni-based MOF composite (C).

addition, the average diameter of nanofibers increased after incorporating the Ni-based MOF into the fibers.

Fig. 4a–c show the EDS-mapping results for the composite. As can be seen, the Ni-based MOF composite was uniformly dispersed on the polymeric matrix. The yellow points highlight the existence of Ni in that location.

Fig. 5 presents a thermal analysis of the β-CDs/Ni-based MOF composite. The thermal analysis approximately began at 40 °C and ended at 550 °C. The first (124 °C) and second temperatures were related to the partial weight loss due to the vanished and evaporation of trapped solvents. A proportional loss with the ascent in temperature was observed at 234 °C, probably due to the decomposition of the linker on the skeleton. The weight loss of the coordinated water dissociation for the nanocomposites was determined at 441 °C. According to these findings, a high thermal stability was noted at increased temperatures.
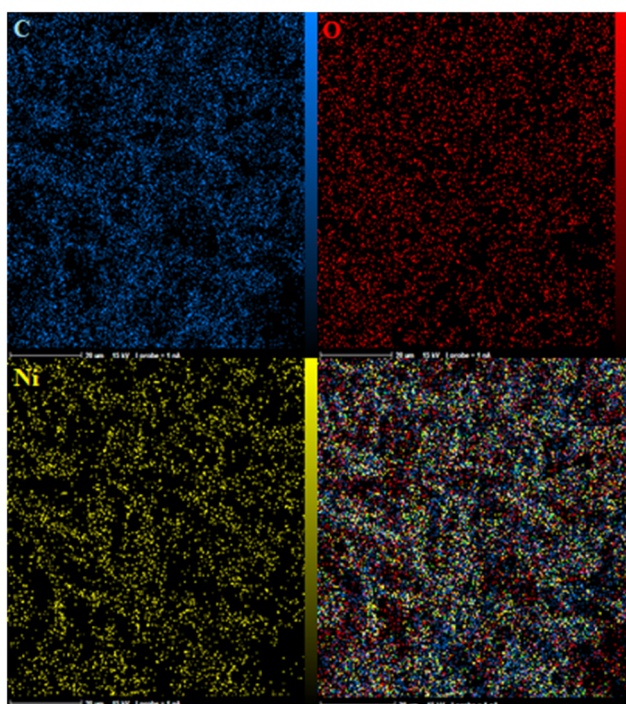
Fig. 6 presents the N_2 adsorption–desorption isotherm of the β-CDs/Ni-based MOF composite, Ni-based MOF, and β-CDs. The N_2 sorption determinations were utilized to measure the physical features, such as pore-size distribution, pore volume, and surface area. Fig. 6a and b display the type IV isotherms for the β-CDs and Ni-based MOF with a clear hysteresis loop. The surface areas were determined to be 1136 m^2 g^{-1} for the Ni-based MOF composite and 849 m^2 g^{-1} for the β-CDs. Based on the observations (Fig. 6c), a type IV isotherm with a type H2 hysteresis loop was found for the β-CDs/Ni-based MOF composite, typically confirming the materials with inkbottle-like pores and a uniform mesoporous structure. The β-CDs/Ni-based MOF composite had the surface area of 2140 m^2 g^{-1}, probably indicating a high porosity and a broad pore opening, which would make this composite one of the best substrates to improve bone-fracture healing.

The Ni-based MOF and β-CDs/Ni-based MOF composite magnetic hysteresis loops were measured in the presence of a magnetic field by VSM. Fig. 7 shows the hysteresis loops of the Ni-based MOF (curve a) and β-CDs/Ni-based MOF composite (curve b) at room temperature. This behavior proved that the Ni-based MOF had super-paramagnetic properties. The Ni-based MOF had a small remanent magnetization (Mr, 0.01479 emu g^{-1}) and coercivity (Hc, 150.0 Oe), which indicated its magnetic behavior and that it showed saturation magnetism (Ms, 0.0821
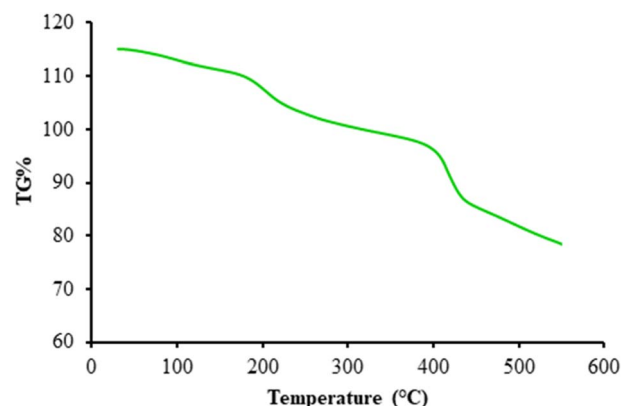

Fig. 4 EDS-mapping of β-CDs/Ni-based MOF composite.

Fig. 5 TGA analysis of β-CDs/Ni-based MOF composite.

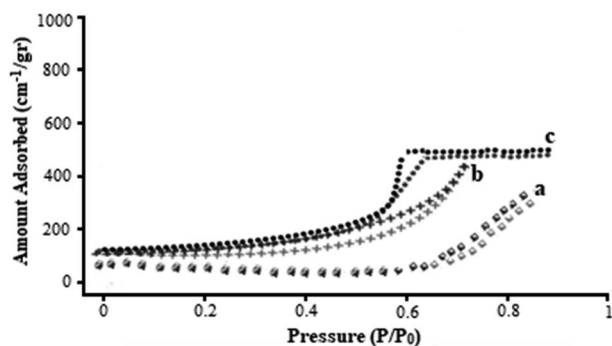**Fig. 6** N_2 adsorption–desorption isotherms β-CDs (a), Ni-based MOF (b), and β-CDs/Ni-based MOF composite (c).

emu g^{-1}). In addition, as shown in Fig. 7 (curve b), its magnetic properties (Mr (0.0082 emu g^{-1}), Hc (100.0 Oe), and Ms (0.0305 emu g^{-1})) decreased with increasing the β-CDs to Ni-based MOF.

The mechanical properties such as tensile modulus, ultimate tensile stress, and ultimate strain, were evaluated for the β-CDs and β-CDs/Ni-based MOF fibrous scaffolds. The tensile properties, Young's modulus, and strain at break are summarized in Table 1 and Fig. 8. The tensile strengths of the β-CDs and β-CDs/Ni-based MOF fibrous scaffolds were around 3.94 ±

0.2 and 2.31 ± 0.1 MPa respectively. The β-CDs blended with Ni-based MOF showed no improvement in the tensile property of the scaffold compared to the β-CDs fibrous scaffold. With regard to the elongation, the blended β-CDs did not reduce the extension ability but maintained the stability of the Ni-based MOF fibrous scaffolds.

3.2. Biocompatibility of the fibrous scaffolds

In regenerative medicine, an ideal scaffold is expected to have high biocompatibility. To study cell activity, the mitochondrial activity of MC3T3-E1 cells on the β-CDs, Ni-based MOF, and β-CDs/Ni-based MOF fibrous scaffolds mats after three days of culture was investigated by the WST-1 method (Fig. 9). In the metabolically active cells, tetrazolium compound is metabolized to formazan and is secreted into the medium. The resulting colorimetric change in the medium can be spectrophotometrically measured to represent the mitochondrial activity of the viable cells. The cell proliferation assay was performed according to ISO-10993-5. According to ISO-10993-5, a cell viability below 40% indicates a material is highly toxic, 60–40% is moderately toxic, between 80% and 60% is weakly toxic, and above 80% is considered to be non-toxic. At day 3 the cell viabilities were above 82%, 87%, and 96% for the β-CDs, Ni-based MOF, and β-CDs/Ni-based MOF fibrous scaffolds mats, respectively ($p < 0.05$). Since the percentage of cell viability for
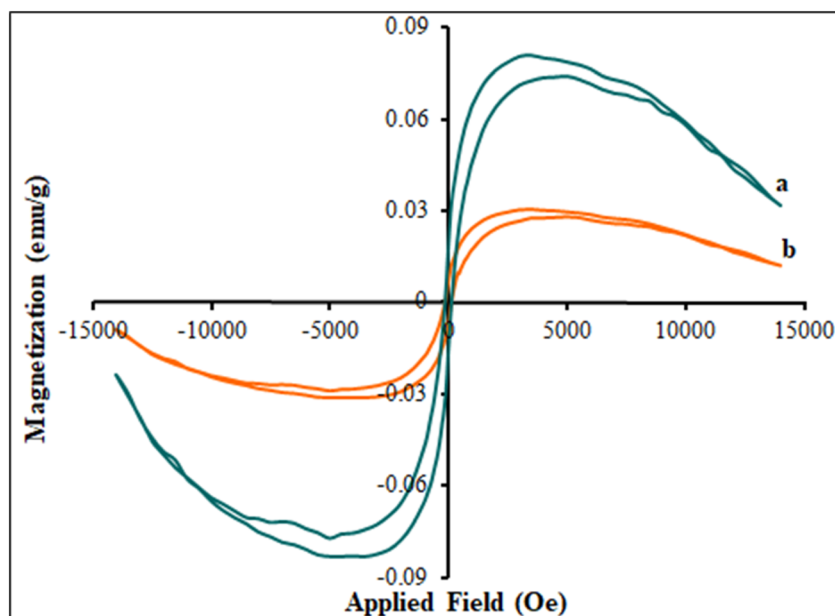

Fig. 7 VSM magnetization curves of Ni-based MOF (a) and β-CDs/Ni-based MOF composite (b).

Table 1 Tensile properties of the electrospun fibrous scaffolds

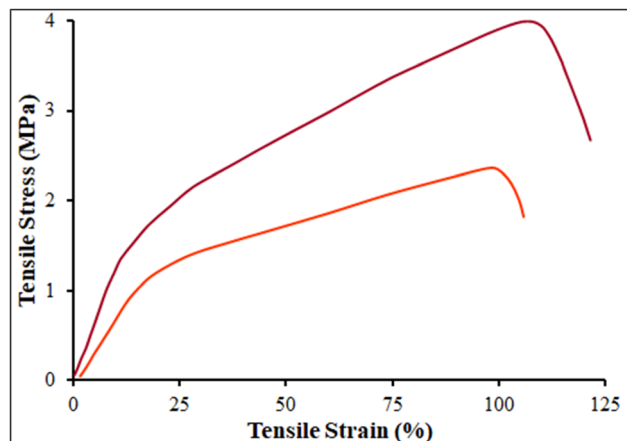| Sample	Tensile strength (MPa)	Young's modulus (MPa)	Strain at break (%)
β-CDs	3.94 ± 0.2	11.25 ± 0.8	121
β-CDs/Ni-based MOF	2.31 ± 0.1	8.37 ± 1.1	106

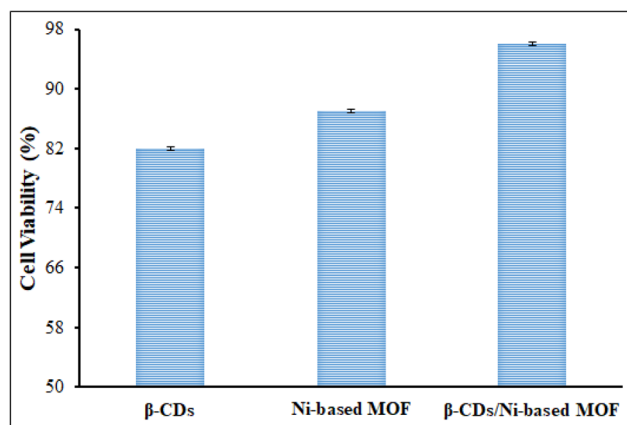**Fig. 8** Stress–strain curve for the β-CDs and β-CDs/Ni-based MOF under tensile loading.

Fig. 9 MC3T3-E1 cell viability (%) of the β-CDs, Ni-based MOF, and β-CDs/Ni-based MOF nanofibrous membranes at day 3 using the WST-1 colorimetric assay.

Fig. 10 Fluorescent microscopy of cells seeded on β-CDs and β-CDs/Ni-based MOF composite scaffolds on days 1, 6, and 12 after cell seeding. Staining: phalloidin-DAPI. Scale bar: 50 μm.

all three compounds was more than 80%, these compounds could be classed as non-toxic. The nature of β-CDs may be one of the factors that caused the high biocompatibility in the fibrous nanostructures. The presence of porosity in this structure could improve the efficiency of the final composition.

3.3. Cell culturing

The two scaffolds of β-CDs/Ni-based MOF composite and β-CDs fabricated in this study were examined with the NHDF cell line. Fig. 10 shows the morphology of NHDF cells co-cultured with different types of scaffolds after 1, 6, and 12 days. With increasing the culture time, the cells grew and proliferated well. The NHDF cell show a normal and well-preserved morphology for a period of 12 days. Only a small number of cells could be observed at day 1. A large amount of cells proliferated and attached to the scaffolds at day 12. On the other hand, the addition of the Ni-based MOF into the β-CDs scaffolds improved cell attachment, showing a well-spread morphology and higher proliferation when
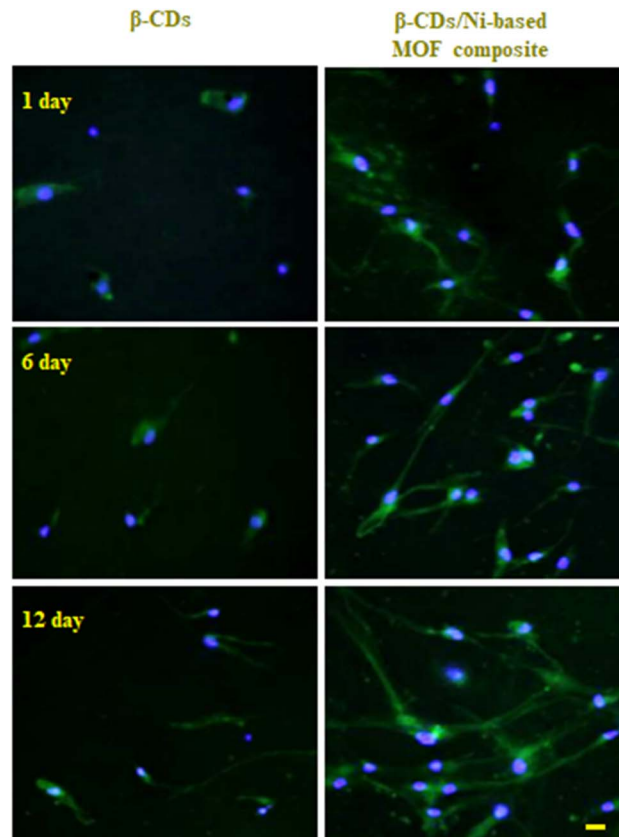
compared to the β-CDs scaffolds alone. Further, the scaffold possessed desirable cytocompatibility and sufficient mechanical strength for bone repair. According to the results, the better porosity of the β-CDs/Ni-based MOF scaffolds is an essential property leading to improved proliferation, and nutrition and oxygen delivery, resulting in more tissue regeneration.

The results obtained were consistent with other reports and show that the modified β-CDs composite exhibited significantly higher bone regeneration. Lee *et al.* demonstrated that modified β-CD with polymer scaffolds promoted significantly higher bone regeneration than unmodified β-CD scaffolds.[28] Du *et al.* indicated that the addition of hydroxyapatite into β-CD-based polyurethane scaffolds improved cell attachment, giving a well-spread morphology and higher proliferation. In addition, this β-CD composite scaffold has the potential to be applied in bone repair and regeneration.[39] In Lukášek *et al.*'s report, a cyclodextrin-enriched composite scaffold revealed better performance in *in vitro* experiments compared with pristine polycaprolactone or polypyrrole-covered polycaprolactone scaffolds.[41] Yi *et al.* indicated that the poly(L-lactide)-β-CD-hydroxyapatite composite possessed a rather large biocompatibility and bioactivity, and it could be a promising candidate as a bone tissue engineering material.[42]

4. Conclusions

The electrospinning process is known to be a suitable method for producing fibrous scaffolds with diverse biological purposes, and hence was applied in this study to construct a β-CDs/Ni-based MOF composite using β-CDs and Ni-based MOF. The Ni-based MOF was confirmed to be present in the β-CDs matrix based on the XRD and FT-IR findings. According to the SEM images, the integration of the Ni-based MOF had no impact on the fibrous shape of the β-CDs. The EDS-mapping images confirmed the uniform dispersion of the Ni-based MOF content in the polymer matrix of the as-fabricated nano-composites. The cytocompatibility of the composite scaffolds was proven *via* their favorable interactions with NHDF cells. The addition of Ni-based MOF into the β-CDs scaffolds improved the cell attachment, giving a well-spread morphology and higher proliferation. Therefore, the as-fabricated β-CDs/Ni-based MOF composite can be suggested to be an impressive scaffold for successful tissue engineering and regeneration medicine owing to the scaffold porosity.

Conflicts of interest

There are no conflicts to declare.

References

1 M. Mallick, R. Prasad Are and A. R. Babu, *Materialia*, 2022, **22**, 101391.
2 J. Gao, L. Feng, B. Chen, B. Fu and M. Zhu, *Composites, Part B*, 2022, **235**, 109758.
3 F. Raquel Maia, A. R. Bastos, J. M. Oliveira, V. M. Correlo and R. L. Reis, *Bone*, 2022, **154**, 116256.
4 J. Venugopa, S. Low, A. Tar Choon, A. Bharath Kumar and S. Ramakrishna, *J. Biomed. Mater. Res., Part A*, 2008, **82**, 408–417.
5 C. Black, J. M. Kanczler, M. C. de Andres, L. J. White, F. M. Savi, O. Bas, S. Saifzadeh, J. Henkel, A. Zannettino, S. Gronthos, M. A. Woodruff, D. W. Hatmacher and R. O. C. Oreffo, *Biomaterials*, 2020, **247**, 119998.
6 X. Wang, C. Li, Y. Zhang, H. Muhammad Ali, S. Sharma, R. Li, M. Yang, Z. Said and X. Liu, *Tribol. Int.*, 2022, **174**, 107766.
7 N. Amiryaghoubi, N. Noroozi Pesyan, M. Fathi and Y. Omidi, *Colloids Surf., A*, 2022, **634**, 127895.
8 X. Cui, C. Li, Y. Zhang, Z. Said, S. Debnath, S. Sharma, H. Muhammad Ali, M. Yang, T. Gao and R. Li, *J. Manuf. Process.*, 2022, **80**, 273–286.
9 S. Wenzhi, W. Dezhou, G. Min, H. Chunya, Z. Lanlan and Z. Peibiao, *Mater. Sci. Eng., C*, 2021, **128**, 112299.
10 J. Zhang, C. Li, Y. Zhang, M. Yang, D. Jia, G. Liu, Y. Hou, R. Li, N. Zhang, Q. Wu and H. Cao, *J. Cleaner Prod.*, 2018, **193**, 236–248.
11 B. M. Min, G. Lee, S. H. Kim, Y. S. Nam, T. S. Lee and W. H. Park, *Biomaterials*, 2004, **25**, 1289–1297.
12 W. Lai, *Mol. Pharm.*, 2021, **18**, 1833–1841.
13 N. Bhattarai, D. Edmondson, O. Veiseh, F. A. Matsen and M. Zhang, *Biomaterials*, 2005, **26**, 6176–6184.
14 W. Lai and W. Wong, *Pharmaceutics*, 2021, **13**, 787–797.
15 J. A. Matthews, G. E. Wnek, D. G. Simpson and G. L. Bowlin, *Biomacromolecules*, 2003, **3**, 232–238.
16 T. Gao, C. Li, M. Yang, Y. Zhang, D. Jia, W. Ding, S. Debnath, T. Yu, Z. Said and J. Wang, *J. Mater. Process. Technol.*, 2021, **290**, 116976.
17 R. Junka and X. Yu, *Mater. Sci. Eng., C*, 2020, **113**, 110981.
18 M. Yang, C. Li, Y. Zhang, D. Jia, R. Li, Y. Hou, H. Cao and J. Wang, *Ceram. Int.*, 2019, **45**, 14908–14920.
19 W. J. Li, K. G. Danielson, P. G. Alexander and R. S. Tuan, *J. Biomed. Mater. Res., Part A*, 2003, **67**, 1105–1114.
20 M. Yang, C. Li, Y. Zhang, D. Jia, X. Zhang, Y. Hou, R. Li and J. Wang, *Int. J. Mach. Tool Manufact.*, 2017, **122**, 55–65.
21 C. Alvarez-Lorenzo, C. A. García-González and A. Concheiro, *J. Controlled Release*, 2017, **268**, 269–281.
22 Y. Zhang, C. Li, H. Ji, X. Yang, M. Yang, D. Jia, X. Zhang, R. Li and J. Wang, *Int. J. Mach. Tool Manufact.*, 2017, **122**, 81–97.
23 X. Ma, N. Zhou, T. Zhang, Z. Guo, W. Hu, C. Zhu, D. Ma and N. Gu, *RSC Adv.*, 2016, **6**, 13129–13136.
24 W. J. Yi, L. J. Li, H. He, Z. Hao, B. Liu, Z. S. Chao and Y. Shen, *New J. Chem.*, 2018, **42**, 14729–14732.
25 W. K. Grier, A. S. Tiffany, M. D. Ramsey and B. A. C. Harley, *Acta Biomater.*, 2018, **76**, 116–125.
26 T. G. B. Deluzio, K. I. Penev and K. Mequanint, *J. Biomater. Tissue Eng.*, 2014, **4**, 957–966.
27 S. Majumdar, X. Wang, S. D. Sommerfeld, J. J. Chae, E. N. Athanasopoulou, L. S. Shores, X. Duan, L. M. Amzel, F. Stellacci and O. Schein, *Adv. Funct. Mater.*, 2018, **28**, 1804076.
28 J. B. Lee, J. E. Kim, D. A. Balikov, M. S. Bae, D. N. Heo, D. Lee, H. J. Rim, D. W. Lee, H. J. Sung and I. K. Kwon, *Macromol. Biosci.*, 2016, **16**, 1027–1038.
29 N. Kaur, V. Kumar and S. R. Dhakate, *SpringerPlus*, 2016, **5**, 483.
30 A. Hamedi, M. Borhani Zarandi and M. R. Nateghi, *J. Environ. Chem. Eng.*, 2019, **7**, 102882.
31 A. Hamedi, A. Anceschi, F. Trotta, M. Hasanzadeh and F. Caldera, *J. Inclusion Phenom. Macrocyclic Chem.*, 2021, **99**, 245–253.
32 Y. Zhang, C. Li, D. Jia, D. Zhang and X. Zhang, *Int. J. Mach. Tool Manufact.*, 2015, **99**, 19–33.
33 A. Hamedi, A. Anceschi, A. Patrucco and M. Hasanzadeh, *J. Drug Targeting*, 2022, **30**, 381–393.
34 Q. Fang, X. Liu, K. Zeng, X. Zhang, M. Zhou and J. Du, *Undergr. Space*, 2022, **7**, 1125–1138, ISSN 2467-9674.
35 A. Hamedi and M. Taheri, *Mol. Cryst. Liq. Cryst.*, 2022, **736**, 103–112.
36 C. Cao, J. Wang, D. Kwok, Z. Zhang, F. Cui, D. Zhao, M. Jun Li and Q. Zou, *Nucleic Acids Res.*, 2022, **50**, D1123–D1130.
37 A. Hamedi, M. Borhani Zarandi, M. Zanetti, F. Caldera, A. Anceschi and M. R. Nateghi, *Int. J. Mol. Sci.*, 2019, **2020**, 5612–5632.
38 G. Sargazi, D. Afzali, N. Daldosso, H. Kazemian, N. Chauhan, Z. Sadeghian, T. Tajerian, A. Ghafarinazari and M. Mozafari, *Ultrason. Sonochem.*, 2015, **27**, 395–402.

39 J. Du, S. Gan, Q. Bian, D. Fu, Y. Wei, K. Wang, Q. Lin, W. Chen and D. Huang, *J. Biomater. Appl.*, 2018, **33**, 402–409.

40 Sh. Jahani, *Anal. Bioanal. Electrochem.*, 2018, **10**, 739–750.

41 J. Lukášek, Š. Hauzerová, K. Havlícková, K. Strnadová, K. Mašek, M. Stuchlík, I. Stibor, V. Jencová and M. Rezanka, *Polymers*, 2019, **11**, 459–460.

42 W. J. Yi, L. J. Li, H. He, Z. Hao, B. Liu, Z. S. Chao and Y. Shen, *New J. Chem.*, 2018, **42**, 14729–14732.